Pergamon

0892-6875(01)00151-0

Minerals Engineering, Vol. 14, No. 11, pp. 1359–1377, 2001

0892-6875/01/$ - see front matter

ENHANCED DISSOLUTION OF MINERALS: STORED ENERGY, AMORPHISM AND MECHANICAL ACTIVATION

D. TROMANS[§] and J.A. MEECH[¶]

§ Department of Metals and Materials Engineering, University of British Columbia, Vancouver V6T 1Z4, British Columbia, Canada. E-mail: des@cmpe.ubc.ca
¶ Department of Mining and Mineral Processing, University of British Columbia, Canada
(Received 12 April 2001; accepted 6 June 2001)

ABSTRACT

A theoretical evaluation of the origin and role of stored energy in the phenomenon of mechanically-activated dissolution of finely milled minerals has been undertaken. The changing mechanical behaviour of minerals with decreasing particle size is examined, leading to the treatment of stored energy in terms of the generation and retention of crystalline imperfections (dislocations) during extended milling. Development of amorphism, and polymorphism, is treated as a direct consequence of decreased periodicity in the crystal lattice that is associated with an increased accumulation of dislocations. Quantitative estimates of stored energy are presented and used to quantify changes in dissolution kinetics in terms of a decreased activation energy of dissolution and hence, an increase in the relative rate of dissolution. © *2001 Elsevier Science Ltd. All rights reserved.*

Keywords
Comminution; grinding; particle size; leaching; reaction kinetics

INTRODUCTION

Mechanical activation is generating interest as a pre-treatment process prior to the leaching of minerals (Baláž, 2000). The process involves prolonged milling to produce finely-ground particles that exhibit enhanced dissolution rates additional to the effects of increased specific surface area on dissolution. A previous theoretical study by the authors (Tromans and Meech, 1999) showed that surface microtopography plays an important role in mechanically-activated dissolution of particles in the micron to sub-micron range, due to the higher rate of reaction at step edges relative to planar surfaces (terraces). The present work is a continuation of our fundamental analysis of mechanical activation effects. In this paper, we are primarily concerned with the influence of stored energy and the development of amorphism (non-periodic regions) in the mineral lattice, both of which have been linked in a general, non-formalised manner to mechanically-activated dissolution (Tkáčová *et al.*, 1993; Baláž *et al.*, 1996, 2000; Welham, and Llewellyn, 1998; Maurice and Hawk, 1999; Baláž, 2000). For completeness, the influence of stored energy on polymorphic transitions is also included in the analysis.

Initially, we characterise the fundamental mechanical behaviour of minerals as particle size decreases and then assess the resulting effects on the generation of imperfections that control stored energy and transitions to amorphous or polymorphous phases. Subsequently, we estimate the increased chemical free energy per mol due to these imperfections and transitions, and apply these results to an analysis of changes in the activation energy and kinetics of dissolution.

PARTICLE SIZE AND MECHANICAL BEHAVIOUR

The classical energy balance studies of Griffith (1920) on the propagation of a small crack (flaw) in an elastically isotropic solid established a functional relationship between the critical tensile stress σ_c for crack propagation and flaw size, (a), having the general form

$$\sigma_c \propto \left[\frac{E\gamma}{a}\right]^{1/2} \tag{1}$$

where E is the tensile elastic modulus and γ is the surface free energy.

Equation (1) was derived on the basis that the rate of elastic strain energy released during crack propagation was equal to the work required to generate new surface area accompanying crack extension. The analysis was conducted for an ideal brittle solid where inelastic atom displacements (plasticity) in the crack tip region were absent. Other workers recognised that such ideal behaviour does not apply to the majority of crack-sensitive materials and the surface energy term in Equation (1) should be replaced by an energy function that accounts for crack-tip plasticity effects (Irwin 1948, Orowan 1955). Such modifications, applicable where crack tip plasticity is confined to a small plastic enclave in an elastic matrix, have led to the recasting of Griffith's ideas in terms of fracture mechanics concepts:

$$K_{IC}(1-\nu^2) = (E\mathcal{G}_{IC})^{1/2}, \tag{2}$$

where K_{IC} is the critical stress intensity for crack propagation under Type I conditions (opening mode), $\mathcal{G}_{IC}$ is the corresponding critical energy release rate per unit area of crack plane (equivalent to 2γ for ideal brittle fracture and $>2\gamma$ for real materials), and ν is Poisson's ratio. [N.B. Inclusion of the $(1-\nu^2)$ term implies plane strain conditions, which is replaced by unity for plane stress conditions.]
The value of K_{IC} has the general form:

$$K_{IC} = Y\sigma_c(a)^{1/2}, \tag{3}$$

where Y is a geometrical factor related to the shape of the crack, *e.g.* Y has the value $(\pi)^{1/2}$ for a straight through internal crack of length $2a$ and the value $2(\pi)^{-1/2}$ for an internal penny-shaped (disc-shaped) crack of radius a (Broek, 1982).

A general feature of crack-sensitive crystalline materials, including minerals, is that they exhibit small amounts of plasticity via dislocation generation and movement during mechanical testing. For example, Gilman (1958) has listed sixteen non-metallic crystals that exhibit dislocation generation (plasticity) during cleavage crack propagation, including minerals such as galena, calcite, gypsum, dolomite and orthoclase. Also, dislocation generation has been detected around hardness test indentations on ceramic single crystals, such as perovskite ($Na_{0.75}WO_3$) and MgO (McColm, 1990).

Application of Equations (2) and (3) to minerals containing a size distribution of flaws (cracks) allows changes in mechanical behaviour to be assessed as particle size decreases during comminution. In particular, these equations show that a decreasing flaw size (a) requires higher tensile stresses for a crack to propagate, $\sigma_c \propto (a)^{-1/2}$. Hence, initial fracture and size reduction of minerals occurs via propagation of the largest flaws at relatively low σ_c. As milled particle size decreases, only small flaws remain and these must be less than the particle diameter. Consequently, increased loading stresses must be imposed to generate further particle fracture via propagation of the remaining flaws. At this point, it is recognised that impact between colliding surfaces during milling produces compressive loads on particles. However, the irregular shape of milled particles ensures that each impact is confined to a local surface area so that a localised elastic strain field is produced that is within a relatively unstrained matrix. The high local compressive stress (σ_P) produced by impact causes an elastic contraction (compression) in the particle parallel to σ_P and a lateral elastic extension normal to σ_P, via Poisson's ratio (ν). Lateral extension is opposed by the relatively unstrained matrix outside the locally impacted region, causing an opposing tensile stress to be

generated in the matrix. These tensile stresses, which can reach values as high as ~$\nu\sigma_P$, are responsible for crack propagation of suitably oriented flaws when:

$$\nu\sigma_P = \sigma_c , \tag{4}$$

As particle size decreases and approaches the micron to sub-micron range where mechanical activation phenomena have been reported (Baláž, 2000), the required σ_c reaches a very large value because of the accompanying small flaw size (*e.g.* a penny-shaped flaw in a 1 μm diameter particle must have $a < 0.5$ μm). The necessary impact stress σ_P for propagation of a penny-shaped flaw is obtained from Eqs. (3) and (4):

$$\sigma_P \approx \frac{K_{IC}}{\nu Y(a)^{1/2}} \approx \frac{K_{IC}}{2\nu}\left(\frac{\pi}{a}\right)^{1/2} \tag{5}$$

Equation (5) can be reset in terms of average particle diameter D by expressing a as a fraction (f) of D:

$$\sigma_P \approx \frac{K_{IC}}{2\nu}\left(\frac{\pi}{fD}\right)^{1/2} \quad \text{or} \quad fD = \pi\left(\frac{K_{IC}}{2\sigma_P\nu}\right)^2 \tag{6}$$

where f is < 0.5.

Analyses by Maurice and Courtney(1990) indicate σ_P reaches several GPa (*e.g.* 2 to 6 GPa) in attrition mills. Typical K_{IC} and ν values for minerals are ~1 to 2 MPa.m$^{1/2}$ (Rummel, 1982) and ~0.25 to 0.3 (Gebrande, 1982), respectively. Combining an upper value of 6 GPa for σ_P with 0.3 for ν, Eq. (6) shows that fD is ~0.24 μm and ~0.97 μm for K_{IC} values of 1 and 2 MPa.m$^{1/2}$, respectively. Hence, a limiting D of the order of 0.5 to 2 μm is reached below which further particle fracture by attrition is unlikely. However, local shear stresses τ generated by impact loading ($\tau \approx \sigma_P / 2$) are still available to promote shape change via particle plasticity (dislocation generation), provided these stresses are of sufficient magnitude. This appears to be the situation in attrition mills where, τ can become so large ($\sigma_P/2$ is ~1 to ~3 GPa) that dislocation generation is likely. Supporting evidence is provided by the studies of Murr and Hiskey (1981) who used transmission electron microscopy to demonstrate that single explosively-driven shock pulses (σ_P) of 1.2 GPa increased the dislocation density of chalcopyrite ($CuFeS_2$) crystals by ~10^2 times, rising to over 10^3 times at 18 GPa.

The preceding fundamental analysis indicates a limiting particle size in the micron to sub-micron range is reached under the high σ_P conditions characteristic of attrition-type milling (or similar milling techniques), and that particle fracture is replaced by increased dislocation activity. The lattice strains associated with an increased number of dislocations are expected to contribute to the "stored energy" associated with finely-milled minerals and to influence the degree of disorder (non-periodicity) or amorphism in the crystal lattice. In addition, or alternatively, the increase in internal energy may promote transitions to less thermodynamically-stable crystalline phases in minerals that exhibit polymorphism.

STORED ENERGY, AMORPHISM AND POLYMORPHISM

Stored energy

The increase in molar Gibbs free energy of milled particles due to dislocations, ΔG_d, is related to changes in molar enthalpy ΔH_d and molar entropy ΔS_d associated with these dislocations:

$$\Delta G_d = \Delta H_d - T\Delta S_d \approx \Delta H_d \tag{7}$$

where T is the temperature (K).

Dislocations are essentially one dimensional (line) imperfections and calculations suggest that their entropy effect is sufficiently small (Cottrell, 1958) that $T\Delta S_d$ becomes negligible with respect to ΔH_d, as indicated in Eq. (7). The value of ΔH_d is determined by the elastic strain energy of all the dislocations, which is composed of linear elastic strains outside the core of each dislocation and a smaller non-linear elastic component within the core. The linear elastic strain energy per unit length of dislocation, ε, contained between the radius of the dislocation core r_c and an outer bounding radius r_b remote from the core is given by Eq. (8) (Cottrell, 1958):

$$\varepsilon \approx \frac{\boldsymbol{b}^2 \mu_S}{4\pi} \ln\left(\frac{r_b}{r_c}\right) \tag{8}$$

where $\boldsymbol{b}$ is the Burgers vector (displacement vector) of the dislocation and μ_S is the elastic shear modulus.

Inclusion of the dislocation core, to provide an expression for the overall strain energy ε_0 per unit length of dislocation, is obtained with sufficient accuracy by replacing r_c by $\boldsymbol{b}/4$ in Eq. (8) (Hirth and Lothe, 1968). The practical limit to r_b will be half the average distance between neighbouring dislocations, which is determined by the dislocation density ρ_d (total length of dislocation lines per unit volume). Thus, $r_b \approx (\rho_d)^{-1/2}/2$ and ε_0 becomes:

$$\varepsilon_0 \approx \frac{\boldsymbol{b}^2 \mu_S}{4\pi} \ln\left(\frac{2(\rho_d)^{-1/2}}{\boldsymbol{b}}\right) \tag{9}$$

Consequently, ΔH_d is equal to $\rho_d \varepsilon_0 M_V$, where M_V is the molar volume of the mineral, allowing ΔG_d to be obtained from Eqs. (7) and (9):

$$\Delta G_d \approx \Delta H_d = (\rho_d M_V)\frac{\boldsymbol{b}^2 \mu_S}{4\pi} \ln\left(\frac{2(\rho_d)^{-1/2}}{\boldsymbol{b}}\right) \tag{10}$$

Equation (10) provides a quantitative estimate of the increase in molar chemical free energy (increase in stored energy) due to dislocations.

Values of M_V, $\boldsymbol{b}$ and μ_S for several oxide and sulphide minerals under ambient conditions (~298 K) are listed in Table 1, together with silicon. Published crystallographic data (PDF, 1995) were used to obtain M_V and $\boldsymbol{b}$, noting that M_V is the molecular weight of the mineral divided by its density. The magnitude of $\boldsymbol{b}$ represents the size of the smallest perfect dislocation capable of maintaining lattice registry (periodicity) above and below the slip plane during motion of the dislocation. The corresponding crystallographic direction of $\boldsymbol{b}$ is included in Table 1.

The value of each μ_S in Table 1 represents an averaged value for polycrystalline aggregates. With the exception of ilmenite and chalcopyrite, they were computed from anisotropic stiffness and compliance constants for single crystals compiled by Hearmon (1979, 1984). Computations were conducted in two ways: 1) from stiffness constants assuming uniform stress in the aggregate, and b) from compliance constants assuming uniform strain in the aggregate. The two values were then averaged. The matrix and analytical procedures required for such computations are outlined by Gebrande (1982) and Wachtman (1996). The μ_S of ilmenite (~90 GPa) was assumed to be similar to that of Ti_2O_3 (94 GPa) because of chemical and structural similarities. The μ_S of chalcopyrite (~30 GPa) was assumed to be similar to that of sphalerite (31.3 GPa) because of structural similarities between their unit cells (Wells,1962).

TABLE 1 Properties of selected oxide and sulphide minerals at ~298K

Mineral	Formula	Structure	*b* (nm)	Direction of *b*	M_V (m^3)	μ_S (Gpa)
Magnetite	Fe_3O_4	Cubic	0.593687	[110]	4.4553 x 10^{-5}	91.3*
Corundum	Al_2O_3	Trigonal	0.4758	[100]	2.556 x 10^{-5}	162*
α-Ti_2O_3	Ti_2O_3	Trigonal	0.5139	[100]	3.1356 x 10^{-5}	94*
Ilmenite	$FeTiO_3$	Trigonal	0.5088	[100]	3.172 x 10^{-5}	~90‡
Rutile	TiO_2	Tetragonal	0.2959	[001]	1.880 x 10^{-5}	112†
α-Quartz	SiO_2	Trigonal	0.4913	[100]	2.268 x 10^{-5}	44.3*
Periclase	MgO	Cubic	0.29776	[110]	1.1241 x 10^{-5}	130.3*
Bunsenite	NiO	Cubic	0.295288	[110]	1.0971 x 10^{-5}	89.8*
Zincite	ZnO	Hexagonal	0.3249	[100]	1.434 x 10^{-5}	46.9*
Cuprite	Cu_2O	Cubic	0.42690	[100]	2.3438 x 10^{-5}	10.3‡
Pyrite	FeS_2	Cubic	0.5417	[100]	2.3932 x 10^{-5}	128*
Pyrargyrite	Ag_3SbS_3	Trigonal	1.104	[100]	9.249 x 10^{-5}	13.9†
Chalcopyrite	$CuFeS_2$	Tetragonal	0.5289	[100]	4.3902 x 10^{-5}	~30‡
β-Molybdenite	MoS_2	Hexagonal	0.3161	[100]	3.205 x 10^{-5}	51.6†
Galena	PbS	Cubic	0.41974	[110]	3.1494 x 10^{-5}	31.5†
Berndite	SnS_2	Trigonal	0.3648	[100]	4.0961 x 10^{-5}	22.6*
Wurtzite	ZnS	Hexagonal	0.382	[100]	2.3824 x 10^{-5}	33.3*
Sphalerite	ZnS	Cubic	0.38226	[110]	2.3783 x 10^{-5}	31.3†
Greenockite	CdS	Hexagonal	0.414	[100]	3.0048 x 10^{-5}	16.9†
Silicon	Si	Cubic	0.3840	[110]	1.2061 x 10^{-5}	66.2*

*Hearmon (1979): †Hearmon (1984): ‡Estimated.

Using Eq. (10) and the data in Table 1, the effect of an increasing dislocation density on stored energy is plotted on logarithmic scales for oxide minerals in Figure 1 and sulphide minerals in Figure. 2. It is clear that an increase in ΔG_d > 1kJ/mol requires a ρ_d > 10^{15} m^{-2}. Undeformed quartz crystals have been reported to exhibit ρ_d values of ~ 10^7 m^{-2}, rising to ~10^{16} m^{-2} after severe deformation (Hobbs *et al.* 1976). Consequently, a ρ_d of ~10^{16} m^{-2} is not unexpected during extended milling of minerals. Examination of Figures 1 and 2 indicates that the resulting ΔG_d will be in the range ~0.3 to 3 kJ/mol, depending on the mineral (*e.g.* ~0.7 kJ/mol for quartz).

Values of ρ_d > 10^{18} m^{-2}, are considered meaningless, and excluded from Figures 1and 2, because dislocations would be so close together (< 1 nm separation) that Eqs. (9) and (10) become invalid.

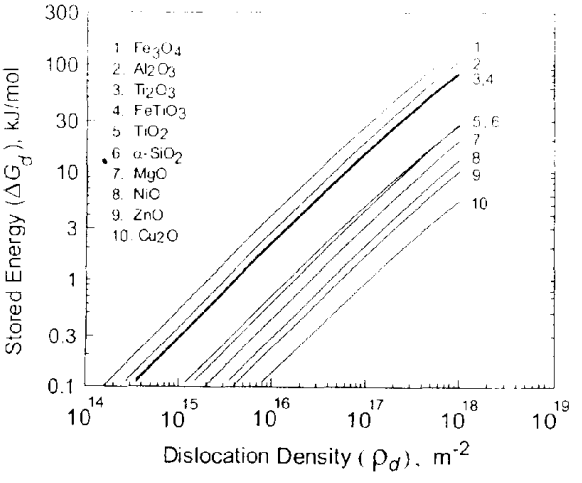

Fig. 1 Effect of dislocation density on stored energy ΔG_d of oxide minerals.

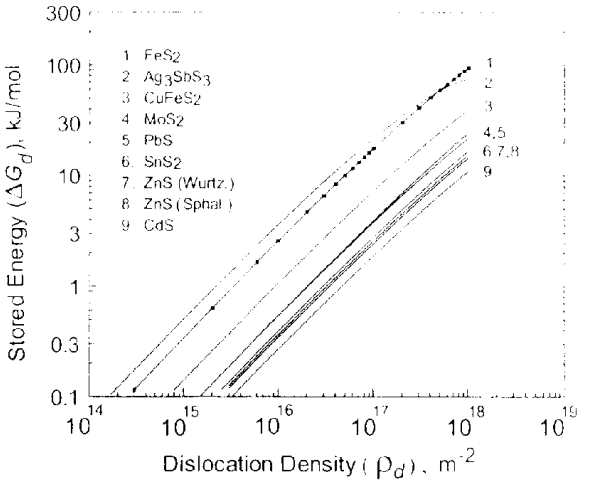

Fig. 2 Effect of dislocation density on stored energy ΔG_d of sulphide minerals. Markers are placed on FeS_2 to distinguish curve from Ag_3SbS_3.

Energy of amorphism

The development of large numbers of dislocations, and their associated strain fields, may lead to an overall decrease in long-range lattice periodicity. This may be interpreted as the formation of a metastable "amorphous phase," because line broadening and disappearance of diffraction peaks takes place on X-ray patterns after extended milling. Estimates of the chemical free energy of amorphous phases, based on structure alone, are difficult because their atom distributions are not readily described. For example, amorphous solids have varying degrees of short-range order requiring quantification in terms of atom distribution (frequency) functions, changes in local geometry and changes in local symmetry (Gaskell, 1991). An alternative thermodynamic approach, developed in the Appendix, is to assume a basic structural similarity between the metastable amorphous phase and the liquid. This approach leads to Eq. (A10), reproduced as Eq. (11) below:

$$(\Delta G_{am-cr})_T = \left(\frac{H_F}{T_m}\right)(T_m - T) \tag{11}$$

where H_F is the enthalpy of fusion at the melting point T_m, and $(\Delta G_{am-cr})_T$ is the estimated maximum change in chemical free energy between the metastable amorphous phase and stable crystalline phase at temperature T.

Estimations of $(\Delta G_{am-cr})_T$ at 298 K and 400 K are listed in Table 2 for the minerals listed in Table 1 where both T_m and H_F data are available (Barin and Platzki, 1995) and for which there are no polymorphous transitions between T and T_m. Note that H_F for chalcopyrite ($CuFeS_2$) is assumed to be ~63 kJ/mol, based on the likelihood that it is approximately twice that of FeS, for which H_F is 31.464 kJ/mol (Barin and Platzki, 1995). This follows from the fact $CuFeS_2$ has two times more atoms per mol than FeS and, therefore, twice as many bonds to break per mol upon melting. Also, H_F for pyrite (FeS_2) is assumed to be ~66 kJ/mol because its stoichiometry and crystal structure symmetry (Wells,1962; PDF, 1995) are identical to those of vaesite (NiS_2), for which H_F is 65.689 kJ/mol (Barin and Platzki, 1995).

If deformation induces the formation of an amorphous phase, it is reasonable to expect the accompanying increase in chemical free energy to be reached when the thermodynamic equality condition of Eq. (12) is satisfied:

$$(\Delta G_{am-cr})_T = \Delta G_d \tag{12}$$

TABLE 2 Estimation of difference in chemical free energy $(\Delta G_{am-cr})_T$ between amorphous and crystalline phases

Mineral	Formula	T_m (K)	H_F (kJ/mol)*	$(\Delta G_{am-cr})_T$, kJ/mol		Equivalent ρ_d at 298 K: $(\Delta G_{am-cr})_T = \Delta G_d$
				T= 298 K	T= 400 K	
Magnetite	Fe_3O_4	1870	138.072	116.07	108.54	~8 x 10^{17} m^{-2}
Corundum	Al_2O_3	2327	111.085	96.859	91.99	~8.5 x 10^{17} m^{-2}
Ilmenite	$FeTiO_3$	1658	90.793	74.474	68.889	~9 x 10^{17} m^{-2}
Rutile	TiO_2	2130	66.944	57.578	54.372	Equality not reached.††
Periclase	MgO	3105	77.822	70.353	67.797	~8.8 x 10^{17} m^{-2}
Bunsenite	NiO	2228	54.393	47.117	44.627	~8.8 x 10^{17} m^{-2}
Zincite	ZnO	2248	54.392	47.182	44.714	Equality not reached.††
Cuprite	Cu_2O	1516.7	64.768	52.042	47.687	Equality not reached.††
Pyrite	FeS_2	1440‡	~66*	52.34	47.67	~4.3 x 10^{17} m^{-2}
Chalcopyrite	$CuFeS_2$	1223‡	~63*	47.65	42.4	~1.4 x 10^{18} m^{-2}
Galena	PbS	1386.5	18.83	14.783	13.398	~5.8 x 10^{17} m^{-2}
Wurtzite	ZnS	1995	10.878	9.2531	8.6969	~5 x 10^{17} m^{-2}
Silicon	Si	1685	50.208	41.328	38.289	Equality not reached.††

*Barin and Platzki (1995); ‡Roine (1999); *Estimated; ††Not reached at ρ_d ~10^{18} m^{-2}.

Comparison of Table 1 with Figures 1 and 2 indicates satisfaction of Eq. (12) requires ρ_d to be in excess of 10^{17} m^{-2}. This is evident by examining the required ρ_d at 298 K in the last column of Table 1. In some cases, such as cuprite, zincite, rutile and silicon the equality condition is not reached at ρ_d ~10^{18} m^{-2}, above which Eq. (10) becomes invalid for estimating ΔG_d, indicating that complete transformation to an amorphous phase by deformation is not possible.

Note that Eq. (12) specifies the condition for which the whole mineral becomes amorphous. Thermodynamically, it does not preclude the possibility that a corresponding mol fraction of mineral is transformed to the metastable amorphous phase when $\Delta G_d < (\Delta G_{am-cr})_1$. For example, when $\rho_d = 10^{17}$ m^{-2}, ΔG_d for rutile is ~4.5 kJ/mol. From Table 2, this corresponds to 7.8% of $(\Delta G_{am-cr})_T$ at 298 K, equivalent to the formation of ~8 mol% amorphous phase. Similarly for zincite, when $\rho_d = 10^{17}$ m^{-2}, ΔG_d is ~1.68 kJ/mol, and corresponds to formation of ~3.6 mol % of amorphous phase.

Energy differences associated with polymorphous transitions

Many minerals exhibit n polymorphous transitions ($n \geq 1$), with each transition having a characteristic transition enthalpy $(H_\pi)_n$ and transition temperature $(T_\pi)_n$. Three minerals in Table 1, α-Ti_2O_3 (n = 1), α-quartz (n = 2) and sphalerite (n = 2), exhibit such transitions. Their $(H_\pi)_n$ and $(T_\pi)_n$ are listed in Table 3. A general method to estimate differences in molar chemical free energy $(\Delta G_{(n+1)-1})_T$ between the metastable $(n+1)$th polymorph and the 1st (most stable) polymorph when both are present at $T < (T_\pi)_{n+1}$ is developed in the Appendix, leading to Eqs. (A11) and (A12). Also, a method to estimate differences in the molar chemical free energy $(\Delta G_{am-1})_T$ between the metastable amorphous phase and the 1st polymorph when both are present at $T < (T_\pi)_{n+1}$ is presented in the Appendix, leading to Eq. (A13). Results of calculations for α-Ti_2O_3, α-quartz and sphalerite, based on Eqs. (A11) to (A13), are listed in Table 3 for T = 298 K.

Following similar arguments leading to Eq. (12), it is reasonable to anticipate that deformation-induced formation of a metastable polymorphous phase is a likely occurrence at $T < (T_\pi)_{n=1}$ when the thermodynamic equality condition of Eq.(13) is satisfied:

$$(\Delta G_{(n+1)-1})_T = \Delta G_d \qquad (13)$$

Also, similar to Eq. (12), deformation-induced formation of the amorphous phase at $T < (T_\pi)_{n-1}$ is expected to occur when the equality condition of Eq. (14) is satisfied:

$$(\Delta G_{am-1})_T = \Delta G_d \tag{14}$$

Calculations of $(\Delta G_{(n+1)-1})_T$ and $(\Delta G_{am-1})_T$, based on Eqs. (A12) and (A13) respectively, are listed in Table 3. Comparison with Figures 1 and 2, and Eq. (10), indicates deformation-induced polymorphous transitions occur at lower ρ_d than those necessary for formation of amorphous phases. For example, complete transformation of α-Ti_2O_3 to β-Ti_2O_3 at 298 K requires $\rho_d = 1.5 \times 10^{15}$ m^{-2}, whereas formation of the amorphous phase requires $\rho_d \approx 1 \times 10^{18}$ m^{-2}. The latter ρ_d is unrealistic and indicates that complete transformation to the amorphous phase is not possible during deformation. Similarly, transformation of sphalerite to wurtzite requires $\rho_d = 6.1 \times 10^{17}$ m^{-2} and complete formation of the amorphous phase in sphalerite requires an unrealistically high $\rho_d \approx 1.6 \times 10^{18}$ m^{-2}. In the case of quartz, transformation of α to β-quartz occurs at $\rho_d = 6.3 \times 10^{15}$ m^{-2}, with transformation from α-quartz to cristobalite occurring at $\rho_d = 2.3 \times 10^{16}$ m^{-2} followed by transformation of α-quartz to the amorphous phase at $\rho_d \approx 2.5 \times 10^{17}$ m^{-2}. Thus, the analyses suggest deformation-induced polymorphous phases are likely to be more prevalent than amorphous phases during milling of polymorphous minerals, probably forming as stacking-type faults in the crystal lattice.

TABLE 3 Estimation of difference in chemical free energy between $(n+1)$th and first polymorph, $(\Delta G_{(n+1)-1})_T$, and between amorphous phase and first polymorph, $(\Delta G_{am-1})_T$

Formula	1st Polymorph $T = 298$ K	n	$(n+1)$th Polymorph	$(H_\pi)_n$ (kJ/mol)†	$(T_\pi)_n$ (K)‡	$(\Delta G_{(n+1)-1})_T$ (kJ/mol)‡ $T = 298$ K	H_F (kJ/mol)†	T_m (K)‡	$(\Delta G_{am-1})_T$ (kJ/mol) $T = 298$ K
Ti_2O_3	α-Ti_2O_3	1	β-Ti_2O_3	1.138	470	0.4165	104.6	2115	90.23
ZnS	Sphalerite	1	Wurtzite	13.024	1293	10.022	10.878	1995	19.275
SiO_2	α-Quartz	1	β-Quarz	0.728	847	0.4719			
		2	Cristobalite	1.996	1079	1.4447	9.566	1996	10.054

†Barin and Platzki (1995)

CHANGES IN ACTIVATION ENERGY OF DISSOLUTION

Principal factors governing the dissolution (leaching) of minerals under conditions where the rate controlling process is transfer of partially solvated species across the aqueous double layer have been discussed in detail previously (Tromans and Meech 1999). Figure 3(a) depicts such a situation for dissolution of an undeformed (unmilled) mineral where the molar chemical free energy of the dissolved (fully solvated) mineral species at the solvation plane is lower than in the mineral surface. As a dissolving species moves across the double layer there is an initial increase in chemical free energy, rising to a peak as it becomes a partially solvated activated complex, then decreasing as it approaches and becomes fully solvated at the solvation plane. The activation energy for dissolution (forward direction) is denoted $\Delta\vec{G}_1$ and that for deposition (reverse direction) is $\Delta\overleftarrow{G}$, where $\Delta\vec{G}_1 < \Delta\overleftarrow{G}$. Based on Arrhenius rate law behaviour, the resulting dissolution rate R_1 (mol.m^{-2}.s^{-1}) is given by Eq. (15),

$$R_1 = \vec{R} - \overleftarrow{R} = A[\exp(-\Delta\vec{G}_1 / RT) - \exp(-\Delta\overleftarrow{G} / RT)] \tag{15}$$

where $\vec{R}$ and $\overleftarrow{R}$ are rates in the dissolution and deposition directions, respectively, A is a rate constant (mol.m^{-2}.s^{-1}), and R is the gas constant (8.3144 J.K^{-1}.mol^{-1}).

The second exponential term in Eq. (15) is negligible with respect to the first during normal milling practice (Tromans and Meech, 1999), so that Eq (15) becomes:

$$R_1 \approx \vec{R} \approx A\exp(-\Delta\vec{G}_1 / RT) \tag{16}$$

The dissolution of a deformed (milled) mineral with stored energy ΔG_d is depicted in Figure 3(b). The molar activation energy of dissolution is decreased from $\Delta\vec{G}_1$ to $\Delta\vec{G}_2$, whereas the peak energy of the activated complex and $\Delta\overleftarrow{G}$ remain unchanged. Thus, from Eq. (16) the dissolution rate R_2 of the deformed mineral becomes:

$$R_2 \approx A\exp\left(\frac{-\Delta\vec{G}_2}{RT}\right) \approx A\exp\left(\frac{\Delta G_d - \Delta\vec{G}_1}{RT}\right) \tag{17}$$

The resulting dissolution rate ratio R_2/R_1 is obtained from Eqs. (16) and (17):

$$R_2 / R_1 \approx \exp(\Delta G_d / RT) \tag{18}$$

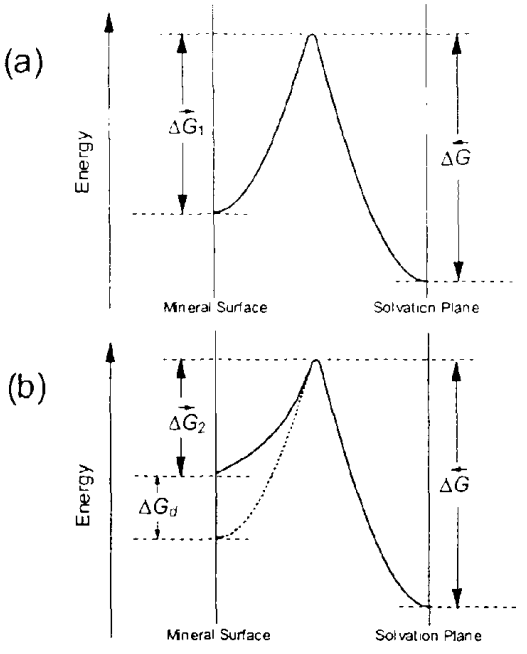

Fig. 3 Schematic diagrams showing changes in activation energy of dissolution: a) Dissolution of undeformed mineral with activation energy of dissolution $\Delta\vec{G}_1$: b) Reduced activation energy of dissolution $\Delta\vec{G}_2$ caused by stored energy ΔG_d.

The effects of different ΔG_d, produced by milling, on dissolution rate ratios at T =298 K and 400 K are summarised in Figure 4, where axes are scaled logarithmically. Evidently, increasing T decreases R_2/R_1 and an increase in chemical free energy of ΔG_d ~0.3 kJ/mol has insignificant effect (~10–13% increase) on the rate ratio. A threefold rate increase requires a ΔG_d of ~3.0 kJ/mol, corresponding to very high $\rho_d > 10^{16}$ m^{-2} in both oxide and sulphide minerals (see Figures 1 and 2). Rate increases >> 50 times are indicated if ΔG_d is > 10 kJ/mol. However, such high dissolution rates may never be achievable in practice, because

subsequent mass transfer controlled processes in the liquid phase will limit the rate of transport of reactants to the mineral surface and/or transport of dissolved products from the surface.

Note that the effects of ΔG_d on dissolution rates may be discussed equally in terms of increased dislocation density or generation of metastable polymorphous and/or amorphous phases, provided the equality conditions of Eqs. (12) to (14) are satisfied. Again, achievable rate increases will be subject to mass transfer limitations so that minerals containing amorphous phase (equivalent to a $\Delta G_d = (\Delta G_{am,\ s})_T$ with ρ_d approaching 10^{18} m^{-2} in Table 2) may not dissolve any faster than milled minerals having lower ΔG_d (lower ρ_d) and no amorphous phase.

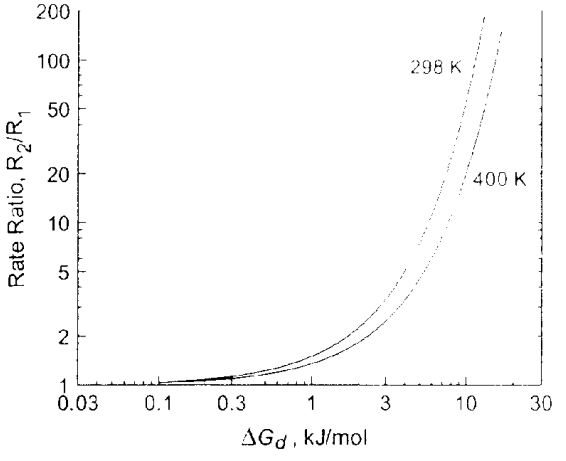

Fig. 4 Effect of change in stored energy ΔG_d on dissolution rate ratio R_2/R_1 at 298 K and 400 K.

A situation of more likely interest in mineral processing is comparison of the dissolution rate R_I of milled particles having an average stored energy of $(\Delta G_d)_I$ with the dissolution rate R_{II} of milled particles having a higher $(\Delta G_d)_{II}$ due to different milling conditions. In. this case, the rate ratio R_{II}/R_I is a modified form of Eq. (18):

$$R_{II}/R_I \approx \exp\left[\frac{(\Delta G_d)_{II} - (\Delta G_d)_I}{RT}\right] \qquad (19)$$

COMPARISON WITH MECHANICAL ACTIVATION PHENOMENA

Structural changes

Few direct observations have been made of crystal defects and structural transformations produced by extended milling. One relevant study by Shen *et al.* (1995) was conducted on shaker-milled Si powders using high-resolution transmission electron microscopy. They observed formation of amorphous regions occupying an average ~15% by volume. At 298 K, 15% of $(\Delta G_{am-1})_T$ for Si corresponds to 6.2 kJ/mol (see Table 2), suggesting this was the average ΔG_d, for which the equivalent ρ_d was near 2.9 x 10^{17} m^{-2} (see Eq. (10) and data in Table 1). The average spacing between dislocations calculated from $(\rho_d)^{-1/2}$ is ~2 nm. The crystallite size in amorphous-free regions of the Si particles was ~3 nm. This is close to, and consistent with the calculated dislocation spacing of 2 nm based on the fraction of amorphous phase.

Tkáčová *et al.* (1993) used X-ray diffraction to measure structural changes related to disorder (loss of periodicity) in a mixed sulphide concentrate during extended milling. Disorder was analysed via changes in

the shape and intensity of X-ray peaks, from which they inferred the percentage of amorphous phase. The concentrate contained chalcopyrite, sphalerite and galena minerals. Their results indicated a limiting percentage of amorphous phase was approached during milling, increasing in the order chalcopyrite (50%) < galena (~65%) < sphalerite (~70%). Such behaviour may be explained in terms of the deformation behaviour of different minerals. As dislocations are generated and move under the shear stress τ produced by impact stresses σ_P on the particles (maximum $\tau \approx \sigma_P/2$), ρ_d increases and causes work hardening. Eventually, further particle deformation becomes negligibly small as work hardening raises the yield stress (τ_y) to $\sigma_P/2$. Under these circumstances, Eq. (20) is an approximate description of the resulting situation for small particles:

$$\tau_y \approx \tau_0 + \alpha_0 \mu_S b(\rho_d)^{1/2} \approx \sigma_P/2 \qquad (20)$$

where τ_0 is the lattice friction stress (Peierls stress) opposing dislocation slip (Hirth and Lothe, 1968) and α_0 is a constant of the order of 0.1 (Cottrell, 1958).

By rearranging Eq.(20) an expression can be obtained for ρ_d as follows:

$$\rho_d = \left(\frac{\sigma_P - 2\tau_0}{2\alpha_0 \mu_S b} \right)^2 \qquad (21)$$

All sulphide particles in the mixed concentrate studied by Tkáčová *et al.* (1993) were subject to the same milling conditions and experienced the same maximum σ_P, as high as, ~6 GPa in attrition mills (Maurice and Courtney, 1990). Since τ_0 is ~$0.1\,\mu_S$ for covalent crystals and less for other types (Hirth and Lothe, 1968), this suggests an upper τ_0 value of ~0.3 GPa for sphalerite, chalcopyite and galena (see Table 1). Hence, τ_0 is negligible relative to σ_P in Eq. (21) so that differences in ρ_d for each milled sulphide are directly related to the product $(\mu_S b)^{-2}$. Lattice disorder arises from an increase in ρ_d which, in turn, is influenced by $(\mu_S b)^{-2}$. Referring to the data in Table 1, $(\mu_S b)^{-2}$ is calculated as 5.765 x 10^{-11}, 10.161 x 10^{-11} and 18.046 x 10^{-11} $Pa^{-2}.m^{-2}$ for chalcopyrite, galena and sphalerite, respectively; the same order in which an increase in the limiting disorder (amorphism) was observed in the mixed concentrate.

Enhanced dissolution effects

The effect of ΔG_d on enhanced dissolution (leaching) rates of minerals is realised only when chemical dissolution is controlled at the surface by transfer of partially solvated complexes across the double layer. There will be little or no influence under conditions where a solid reaction product film (passivating layer) forms on the mineral surface or where dissolution is controlled by mass transport in the liquid phase, the latter situation being typified by an activation energy of ~17 kJ/mol (Tromans and Meech, 1999).

Oxidative leaching of chalcopyrite ($CuFeS_2$) is an example of a system where passivation effects may occur, usually attributed to sulphur films and/or intermediate decomposition products of the mineral (Jones and Peters, 1976; Murr and Hiskey, 1981; Yin *et al.*, 2000). However, Murr and Hiskey (1981) have reported on the leaching of chalcopyrite in a sulphuric acid/dichromate solution at 323 K wherein no passivation was observed and an activation energy of 50 kJ/mol was measured: a characteristic of chemically controlled dissolution. Moreover, they compared dissolution rates of mineral fractions obtained from chalcopyrite milled from natural state crystals (ρ_d ~10^{11} m^{-2}) with similar size fractions milled from crystals shock-loaded at 18 GPa (ρ_d ~10^{15} m^{-2}), where ρ_d was determined by conventional transmission electron microscopy (CTEM). Final particle fractions were –48+65 mesh (250–210 μm) and –100+150 mesh (125–100 μm), which, from Eqs. (5) and (6), were sufficiently large that particle fracture only, with no deformation, was expected during milling. Hence, if ρ_d remained unchanged throughout milling, the shock-loaded and milled material (initial ρ_d ~10^{15} m^{-2}) ought to exhibit a higher dissolution rate than

crystals milled in the natural state (initial ρ_d ~10^{11} m^{-2}). Such anticipated behaviour was observed, dissolution being 1.5 to 2 times higher for crystals milled after shock loading at 18 GPa relative to milled natural crystals. However, the rate ratio was significantly higher than that predicted (~1.05) from Eqs. (10) and (19). A possible explanation for this dicrepancy is that ρ_d for the shock loaded crystals was larger than ~10^{15} m^{-2} reported by Murr and Hiskey (1981). Examination of the published CTEM micrograph of their shock-loaded crystal shows regions where dislocation images are so close together as to be indistinguishable from each other. The CTEM image of a single dislocation usually has a width of 10 nm (strain field effects). Hence if dislocations are so close as to be indistinguishble, their separation is ~10 nm (or less), corresponding to a ρ_d of at least ~10^{16} m^{-2}. Under these circumstances Eqs.(10) and (19) predict a higher dissolution rate ratio of ~1.5, consistent with the observations

Welham and Llewellyn (1998) reported increased leaching rates of ilmenite in sulphuric acid after extended milling. The activation energy of dissolution was reduced from within the range ~70 to ~80 kJ/mol (slow chemical dissolution control) to near ~15 kJ/mol (faster mass transport control) and corresponded to an overall decrease in activation energy of ~60 kJ/mol. From the data for ilmenite in Figure 1, this activation energy decrease (equivalent to a required ΔG_d of ~60 kJ/mol) is readily achieved with a ρ_d of 7 x 10^{17} m^{-2} or, from Table 2, by formation of an amorphous phase where $(\Delta G_{am-cr})_T$ is ~70 kJ/mol.

Microtopography and stored energy

Previous theoretical work has shown that surface microtopography significantly influences the dissolution of particles in the micron to sub-micron range (Tromans and Meech, 1999). The activation energy of dissolution from surface sites at the edges of steps was estimated to be approximately ~20% less than dissolution from surface sites at terraces, leading to a higher dissolution rate at steps. A high density of surface steps arising from particle fracture and cleavage during milling supplies a surface with a large fraction of step sites, leading to an overall increase in the rate of particle dissolution. When deformation-induced stored energy ΔG_d is present, the activation energy for dissolution is also reduced, as shown in Figure 3b and Eq. (17). This reduction applies to all types of dissolution sites, including steps and terraces. Thus, stored energy and microtopography act in synergy to promote enhanced mineral dissolution when both effects are present.

CONCLUSIONS

Theoretical analyses of fine particle behaviour with particular reference to oxide and sulphide minerals, lead to the following conclusions:

1. A limiting particle size in the micron to sub-micron range is reached during extended grinding with attrition-type mills, after which particle fracture is replaced by particle deformation. This limiting particle size is controlled by the fracture toughness of the mineral and the impact loading stresses.

2. Deformation-induced changes in the dislocation density of minerals are quantitatively related to an increase in stored energy. Dislocation densities of ~10^{16} m^{-2} are required to produce a stored energy of ~0.3 to ~3 kJ/mol, depending on the mineral.

3. A deformation-induced amorphous phase produces an increase in stored energy ranging from ~10 to ~100 kJ/mol at 298 K, depending on the mineral. This increase is equivalent to energy changes produced by dislocation densities in excess of 10^{17} m^{-2}.

4. Stored energy associated with a deformation-induced polymorphous phase is much lower than for an amorphous phase.

5. Thermodynamically, stored energy effects may be considered either in terms of lattice disorder related to dislocation density and/or that due to the production of a particular fraction of amorphous (and polymorphous) phase.

6. The activation energy of dissolution is decreased by an amount directly related to the change in stored energy when dissolution is controlled by transfer of partially solvated species across the aqueous double layer,. The resulting effect is an increased dissolution rate (mechanically-activated dissolution). A stored energy increase of ~3 kJ/mol produces a threefold increase in dissolution rate at 298 K.

APPENDIX

Estimated chemical free energy of amorphous phase G_{am}

The amorphous phase is thermodynamically unstable, relative to the crystalline phase, and estimation of its free energy is based upon the hypothetical behaviour of the amorphous phase if it could be preserved below and up to the melting point. Calculation procedures utilise absolute values of the standard state molar values of the Gibbs free energy (G), enthalpy (H) and entropy (S) of single species (see Barin and Platzki, 1995), where subscripts *am*, *cr* and *liq* denote amorphous, crystalline and liquid phases, respectively. Estimation of the maximum value of G_{am} is based on the following conditions:

1. The amorphous phase is treated as a glass-type solid where the atom disorder is similar to that of the liquid phase, except that the atom positions are fixed (apart from thermal vibrations) and unable to undergo long range diffusion movements characteristic of liquids.

2. The T-dependent variations of the molar heat capacities C_P of the corresponding amorphous and crystalline solids are assumed to be similar. This follows from condition **1** and is supported by observed similarities in C_P behaviour between corresponding crystalline and amorphous glass phases in glass-forming minerals, *e.g.*, anorthite, diopside, amphibole and quartz in Figure A1. The C_P data were obtained from Perry *et al.* (1984).

3. At all T, $S_{am} > S_{cr}$. This is consistent with the general concept that the entropy of a disordered solid phase must always be larger than its crystalline counterpart.

4. The value of S_{am} must have a finite value at 0 K. This follows from condition **3** together with the thermodynamic requirement that S_{cr} for a perfect crystal is zero at 0 K (Barin and Platzki, 1995).

The basic thermodynamic equation for the absolute Gibbs free energy of a single species is given by Eq. (A1):

$$G = H - TS \qquad \text{(A1)}$$

At the melting point of the crystal, T_m, thermodynamic equilibrium requires $(G_{cr})_{T_m} = (G_{liq})_{T_m}$ leading to Eq. (A2):

$$(G_{cr})_{T_m} = (H_{cr})_{T_m} - T_m(S_{cr})_{T_m} = (G_{liq})_{T_m} = (H_{liq})_{T_m} - T_m(S_{Liq})_{T_m} = (H_{cr})_{T_m} + H_F - T_m(S_{liq})_{T_m} \qquad \text{(A2)}$$

where H_F is the molar enthalpy of fusion for the crystal/liquid phase transition and $(H_{cr})_{T_m} + H_F = (H_{liq})_{T_m}$.

From Eq. (A2), it is evident that:

$$T_m(S_{liq})_{T_m} = T_m(S_{cr})_{T_m} + H_F \qquad \text{(A3)}$$

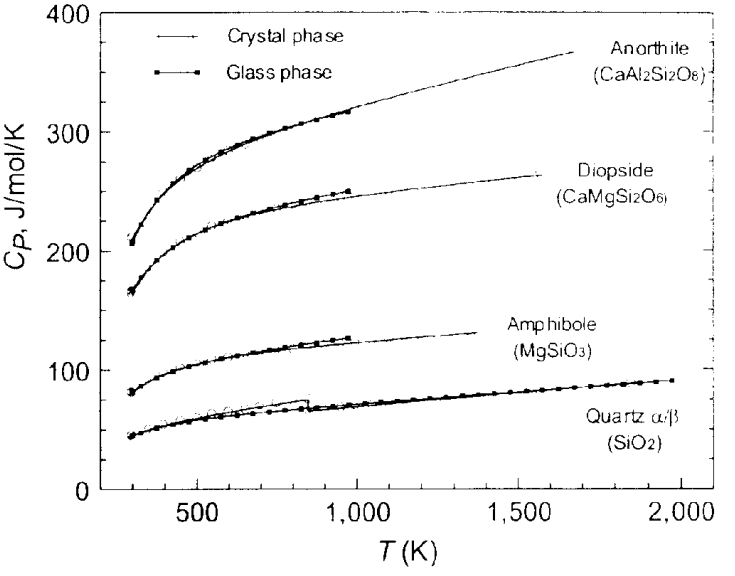

Fig. A1 Temperature dependence of molar heat capacity C_p of crystalline phase and glass phase of several minerals. Data from Perry *et al.* (1984).

After applying condition **1**, which requires the entropy of the amorphous phase at T_m to be the same as the liquid phase, $(S_{am})_{T_m} = (S_{liq})_{T_m}$, Eq. (A3) leads to:

$$(S_{am})_{T_m} = (S_{cr})_{T_m} + \frac{H_F}{T_m} \tag{A4}$$

The entropy of a single species at any temperature T is related to that at another temperature, such as T_m, via Eq. (A5):

$$(S)_T = (S)_{Tm} + \int_{T_m}^{T} \frac{C_P}{T} \partial T \tag{A5}$$

Therefore, applying condition **2** (T-dependent variation of C_P is the same for the crystalline and amorphous phases), it is obvious from Eqs. (A4) and (A5) that $(S_{am})_T > (S_{cr})_T$ at all T, which meets conditions **3** and **4.**

The general thermodynamic relationship relating the free energy G_{T_2} of a single species at temperature T_2 to the free energy G_{T_1} of the species at T_1 is given by Eq. (A6):

$$(G)_{T_2} = (G)_{T_1} + \int_{T_1}^{T_2} C_P \partial T - (T_2 - T_1) S_{T_1} - T_2 \int_{T_1}^{T_2} \frac{C_P}{T} \partial T \tag{A6}$$

Applying Eq. (A6) to the amorphous and crystalline phases at T and T_m, where $T < T_m$, leads to Eqs. (A7) and (A8):

$$(G_{cr})_T = (G_{cr})_{T_m} + \int_{T_m}^{T} C_P \partial T - (T - T_m)(S_{cr})_{T_m} - T \int_{T_m}^{T} \frac{C_P}{T} \partial T \tag{A7}$$

$$(G_{am})_T = (G_{am})_{T_m} + \int_{T_m}^{T} C_P \partial T - (T - T_m)(S_{am})_{T_m} - T \int_{T_m}^{T} \frac{C_P}{T} \partial T \qquad \text{(A8)}$$

Thermodynamic equilibrium at T_m requires $(G_{cr})_{T_m} = (G_{liq})_{T_m} = (G_{am})_{T_m}$. Thus, after applying condition **2** relating to similarity of C_P, subtraction of Eq. (A7) from (A8) yields (A9):

$$(G_{am})_T - (G_{cr})_T = (\Delta G_{am-cr})_T = (T_m - T)\{(S_{am})_{T_m} - (S_{cr})_{T_m}\} \qquad \text{(A9)}$$

where $(\Delta G_{am-cr})_T$ is the difference in molar free energy between the amorphous and crystalline solids at temperature T:

Inserting Eq. (A4) into Eq. (A9) leads to the estimated value of $(\Delta G_{am-cr})_T$:

$$(\Delta G_{am-cr})_T = \left(\frac{H_F}{T_m}\right)(T_m - T) \qquad \text{(A10)}$$

from which $(G_{am})_T$ is readily calculated from known values of $(G_{cr})_T$.

Estimated chemical free energy difference between polymorphous phases

Many minerals exhibit polymorphous phases having identical chemical stoichiometry and different crystal structures (*e.g.* the wurtzite and sphalerite polymorphs of ZnS in Table1). Similar to solid–liquid transformations, there is an equilibrium transition temperature T_π below which one polymorph (phase 1) is most thermodynamically stable and above which the other (phase 2) is most stable. If both polymorphs are present at $T < T_\pi$, there will be a difference in molar chemical free energies $(\Delta G_{2-1})_T$ between the phases at T. If the temperature-dependent behaviour of C_P is closely identical in both phases, analogous arguments to those leading to Eq. (A10) may be applied to $(\Delta G_{2-1})_T$ to produce Eq. (A11):

$$(\Delta G_{2-1})_T = \left(\frac{H_\pi}{T_\pi}\right)(T_\pi - T) \qquad \text{(A11)}$$

where H_π is the enthalpy of transition from phase 1 to phase 2 at T_π.

The validity of Eq. (A11) may be tested by examining the thermodynamic behaviour of sphalerite and wurtzite polymorphs of ZnS, where T_π = 1293 K and H_π = 13.024 kJ/mol (Barin and Platzki, 1995). Sphalerite is the most stable phase below T_π. However, both phases may be present at $T < T_\pi$. The T-dependent C_P data reported by Barin and Platzki (1995), shown in Figure A2, confirm that both polymorphs exhibit almost identical C_P behaviours, as required for Eq. (A11). After inserting T_π and H_π values for ZnS into Eq. (A11), and denoting sphalerite as phase 1 and wurtzite as phase 2, $(\Delta G_{2-1})_T$ is 10.022 kJ/mol at = 298 K, and 8.995. kJ/mol at 400 K. Absolute values of G listed by Barin and Platzki (1995) for sphalerite (G_{sph}) are –222.373 and –228.975 kJ/mol at 298 K and 400 K, respectively. Corresponding G values for wurtzite (G_w) are –212.107 and –219.678 at 298 K and 400 K, respectively. Subtraction of G_{sph} from G_w yields $(\Delta G_{2-1})_T$ values of 10.266 kJ/mol at 298 K, and 9.297 kJ/mol at 400 K, which are within 2.38% and 3.25% respectively of the estimates obtained from Eq. (A11).

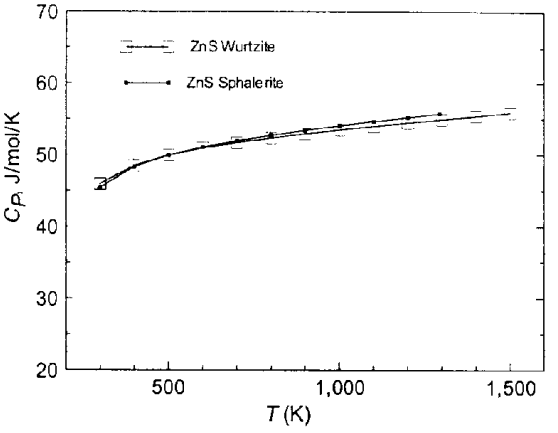

Fig. A2 Temperature dependence of molar heat capacity C_P of sphalerite and wurtzite phases of ZnS. Data from Barin and Platzki (1995).

If n polymorphous transitions occur with increasing T, consistent with $n+1$ polymorphs, Eq.(A11) may be written in a more general form:

$$(\Delta G_{(n+1)-1})_T = \sum_{n=1}^{n=n} \left(\frac{(H_\pi)_n}{(T_\pi)_n} \right) [(T_\pi)_n - T] \tag{A12}$$

where $(H_\pi)_n$ is the enthalpy of the nth polymorphous transition at temperature $(T_\pi)_n$, $(\Delta G_{(n+1)-1})_T$ is the difference in chemical free energy between the $(n+1)$th and first polymorph, and T is below the first transition temperature (*i.e.* $T < (T_\pi)_{n=1}$).

Note that when n allotropic transitions occur with increasing T, H_F corresponds to the enthalpy of fusion for the $(n+1)$th polymorph. Consequently, the estimated difference in chemical free energy $(\Delta G_{am-1})_T$ between the amorphous phase and first polymorph at $T < (T_\pi)_{n=1}$ is obtained from a combination of Eqs. (A10) and (A12):

$$(\Delta G_{am-1})_T = \sum_{n=1}^{n=n} \left(\frac{(H_\pi)_n}{(T_\pi)_n} \right) [(T_\pi)_n - T] + \left(\frac{H_F}{T_m} \right) (T_m - T) \tag{A13}$$

LIST OF SYMBOLS

A	Rate constant (mol.m^{-2}.s^{-1}).
C_P	Molar heat capacity (J.mol^{-1}.K^{-1}).
D	Average particle diameter (m).
E	Tensile elastic modulus (Pa).
G	Standard (absolute) chemical free energy of single species (J/mol).
G_{am}, G_{cr}, G_{liq}	G for amorphous, crystalline and liquid phase, respectively (J/mol).
$\mathcal{G}_{IC}$	Critical strain energy release rate at fracture (J/m^2).
H	Standard (absolute) enthalpy of single species (J/mol).
H_{am}, H_{cr}, H_{liq}	H for amorphous, crystalline and liquid phase, respectively (J/mol).
H_F	Enthalpy of fusion (J/mol).
H_π	Enthalpy of polymorphous phase transition at T_π (J/mol).
$(H_\pi)_n$	Enthalpy of nth polymorphous phase transition at $(T_\pi)_n$ (J/mol).

K_{IC}	Critical stress intensity at particle fracture ($Pa.m^{1/2}$).
M_V	Molar volume (m^3).
R	Gas constant (8.3144 $J.K^{-1}.mol^{-1}$).
R_1	Resulting dissolution rate with activation energy ($mol.m^{-2}.s^{-1}$).
R_2	Resulting dissolution rate with activation energy $\Delta\vec{G}_2$ ($mol.m^{-2}.s^{-1}$)
R_I	Resulting dissolution rate with stored energy $(\Delta G_d)_I$ ($mol.m^{-2}.s^{-1}$).
R_{II}	Resulting dissolution rate with stored energy $(\Delta G_d)_{II}$ ($mol.m^{-2}.s^{-1}$).
$\vec{R}$	Forward rate (dissolution, $mol.m^{-2}.s^{-1}$).
$\overleftarrow{R}$	Reverse rate (deposition, $mol.m^{-2}.s^{-1}$).
S	Standard (absolute) entropy of single species ($J.mol^{-1}.K^{-1}$).
S_{am}, S_{cr}, S_{liq}	S for amorphous, crystalline and liquid phase, respectively ($J.mol^{-1}.K^{-1}$).
T	Temperature (K).
T_m	Temperature at melting (fusion) point (K).
T_π	Equilibrium temperature of polymorphous phase transition (K).
$(T_\pi)_n$	Equilibrium temperature of nth polymorphous phase transition (K).
Y	Geometrical factor related to crack shape.
ΔG	Free energy difference (J/mol).
ΔG_d	Increase in molar free energy (stored energy) due to dislocations (J/mol).
$(\Delta G_d)_I$	Increase in ΔG_d for condition I (J/mol)).
$(\Delta G_d)_{II}$	Increase in ΔG_d for condition II (J/mol)).
$(\Delta G_{am-cr})_T$	ΔG between amorphous and crystal phase at T (J/mol).
$(\Delta G_{2-1})_T$	ΔG between polymorphous phases 2 and 1 at T (J/mol).
$(\Delta G_{(n+1)-1})_T$	ΔG between $(n+1)$th and first polymorphous phase at T (J/mol).
$\Delta\vec{G}_1$	Activation energy for dissolution (forward direction, J/mol).
$\Delta\vec{G}_2$	Activation energy for dissolution with stored energy ΔG_d (J/mol).
$\Delta\overleftarrow{G}$	Activation energy for deposition (reverse direction, J/mol)
ΔH_d	Enthalpy increase due to dislocations (J/mol)
ΔS_d	Entropy increase due to dislocations ($J.mol^{-1}.K^{-1}$).
a	Flaw size (m).
$\boldsymbol{b}$	Burgers vector of dislocation (m).
f	A fraction < 0.5.
n	Number of polymorphous transitions.
r_b	Outer bounding limit (radius) of strain field around a dislocation (m).
r_c	Radius of dislocation core.

Greek symbols

α_0	A constant with an approximate value of 0.1.
ε	Strain energy per unit length of dislocation excluding core energy (J/m).
ε_0	Strain energy per unit length of dislocation including core energy (J/m).
γ	Surface free energy (J/m^2).
μ_S	Elastic shear modulus (Pa).
ν	Poisson's ratio.
ρ_d	Dislocation density (m^{-2}).
σ_c	Critical tensile stress for fracture (Pa)
σ_P	Maximum impact stress (Pa).
τ	Shear stress (Pa).
τ_0	Lattice friction stress (Pa).
τ_y	Shear stress at yielding (Pa).

ACKNOWLEDGEMENTS

The authors wish to thank the Natural Sciences and Engineering Research Council of Canada (NSERC) for financial support.

REFERENCES

Baláž, P., Mechanical activation in technology of metals extraction, *Metall*, 2000 **54(4)**, 190–195.

Baláž, P., Ficeriová, J., Šepelák, V. and Kammel, R., Thiourea leaching of silver from mechanically activated tetrahedrite. *Hydrometallurgy*, 1996 **43**, 367–377.

Baláž, P., Boldižárová, E., Achimovičová, M. and Kammel, R., Leaching and dissolution of a pentlandite concentrate pretreated by mechanical activation. *Hydrometallurgy*, 2000 **57**, 85–96.

Barin, I. and Platzki, G., *Thermochemical data of pure substances*, 1995, 3rd Edition (Vol. I and II), VCH Publishers, Inc., New York, NY.

Broek, D., *Elementary engineering fracture mechanics*, 1982, 3rd Edition, Martinus Nijhoff Publishers, The Hague, Netherlands.

Cottrell, A.H., *Dislocations and plastic flow in crystals*, 1958, Oxford University Press, London, UK, pp. 37–41, 154–155.

Gaskell, P.H., Models for the structure of amorphous solids. In *Materials Science and Technology, Vol. 9, Glasses and Amorphous Materials*, ed. J. Zarzycki, VCH Publishers Inc., New York, NY, 1991, pp. 175–278.

Gebrande, H., Elastic wave velocities and constants of elasticity of rocks and rock forming minerals. In *Landolt–Börnstein Tables, Group V, Vol. 1b*, ed. G. Angenheister, Springer-Verlag, Berlin, 1982, pp. 1–98.

Gilman, J.J., Creation of cleavage steps by dislocation. *Transactions of the Metallurgical Society of AIME*, 1958, **212**, 310–315.

Griffith, A.A., The phenomena of rupture and flow in solids. *Philosophicaal Transactions of the Royal Society*, 1920, **A221**, 168–198.

Hearmon, R.F.S., The elastic constants of crystals and other anisotropic materials. *In Landolt–Börstein Tables, Group III, Vol 11*, eds., K.-H. Hellwege and A.M. Hellwege, Springer-Verlag, Berlin, 1979, pp. 1–244.

Hearmon, R.F.S The elastic constants of crystals and other anisotropic materials. *In Landolt–Bornstein Tables, Group III, Vol 18*, eds. K-H. Hellwege and A.M. Hellwege, Springer-Verag, Berlin, 1984, pp. 1–140.

Hobbs, B.E., Winthrop, D.M. and Williams, P.E., *An outline of structural geology*, 1976, John Wiley and Sons Inc., New York, NY, pp. 82–88.

Hirth, J.P. and Lothe, J., *Theory of dislocations*, 1968, McGraw-Hill, Inc., New York, NY, pp. 62–63, 211 212, 228.

Irwin, G., Fracture dynamics. *Transactions of the American Society for Metals*, 1948 **40a**, 147–166.

Jones, D.L. and Peters, E., The leaching of chalcopyrite with ferric sulfate and ferric chloride. In *Extractive metallurgy of copper, Vol.2*, eds. J.C. Yannopoulos and J.C. Agarwal, TMS-AIME, New York, NY, 1976, 633–653.

Maurice, D.R. and Courtney, T.H., The physics of mechanical alloying; A first report. *Metallurgical Transactions A*, 1990, **21A**, pp. 289–303.

Maurice, D. and Hawk, J.A., Ferric chloride leaching of a mechanically activated pentlandite–chalcopyrite concentrate. *Hydrometallurgy*, 1999 **52**, 289–312.

McColm, I.J., *Ceramic Hardness*, 1990, Plenum Press, New York, NY, pp. 66–69.

Murr, L.E. and Hiskey, J.B., Kinetic effects of particle-size and crystal dislocation density on the dichromate leaching of chalcopyrite. *Metallurgical Transactions B*, 1981. **12B**, 255–267.

Orowan, E., Energy criteria of fracture. *Welding Journal*, 1955, **34**, 157s–160s.

PDF—Powder Diffraction File, PCPDFWIN, JCPDS—International Center for Diffraction Data, Swarthmore, PA, 1995.

Perry, R.H., Green, D.W. and Maloney, J.O. (Eds.), *Perry's chemical engineers' handbook*, 1984, Sixth Edition, McGraw-Hill, New York, NY, pp. 3–129 to 3–135.

Roine, A., *HSC Chemistry for Windows, Version 4.0, Chemical Reaction and Equilibrium Software with Extensive Thermochemical Database*, 1999, Outokompu Research Oy, Pori, Finland.

Rummel, F., Fracture and flow of rocks and minerals: Strength and deformability.. In *Landolt–Börnstein tables, Group V, Vol. 1b*, ed. G. Angenheister, Springer-Verlag, Berlin, 1982, pp. 141–194.

Shen, T.L., Koch, C.C., McCormick, T.L., Nemanich, R.J., Huang, J.Y. and Huang, J.G., The structure and property characteristics of amorphous/nanocrystalline silicon produced by ball milling. *J. Materials Research*, 1995, **10 (1)**, 139–148.

Tkáčová, K., Baláž, P., Mišura, B., Vigdergauz, V.E. and Chanturiya, V.A., Selective leaching of zinc from mechanically activated complex Cu–Pb–Zn concentrate. *Hydrometallurgy*, 1993, **33**, 291–300.

Tromans, D., and Meech, J.A., Enhanced dissolution of minerals: Microtopography and mechanical activation. *Minerals Engineering*, 1999, **12(6)**, 609–625.

Wachtman, J.B., *Mechanical properties of ceramics*, 1996, John Wiley and Sons, Inc., New York, NY, pp. 1–35.

Welham, N.J. and Llewellyn, D.J., Mechanical enhancement of the dissolution of ilmenite, *Minerals Engineering*, 1998 **11(9)**, 827–841.

Wells, A.F., *Structural inorganic chemistry*, 1962 Oxford University Press, London, UK, pp. 520–521, 531–532.

Yin, Q., Vaughan, D.J., England, K.E.R., Kelsall, G.H. and Brandon, N.P., Surface oxidation of chalcopyite ($CuFeS_2$) in alkaline solutions. *J. Electrochemical Soc.*, 2000 **147(8)**, 2945–2951.

Correspondence on papers published in *Minerals Engineering* is invited by e-mail to bwills@min-eng.com